IRIS RECOGNITION SYSTEM USING GABOR WAVELET

Kriti Masih[*1], C.Chandrakar[2], Monisha Sharma[3]
[*1,2,3]Shankracharya Institute of Technology, Bhilai, Chhattisgarh

Abstract

A new approach for personal identification based on iris recognition is presented in this paper. The body of this paper details the steps of iris recognition, including image preprocessing, feature extraction and classifier design. The proposed algorithm uses a bank of Gabor filters to capture both local and global iris characteristics to form a fixed length feature vector. Iris matching is based on the weighted Euclidean distance between the two corresponding iris vectors and is therefore very fast. Experimental results are reported to demonstrate the performance of the algorithm.

Keywords - Iris recognition, Feature extraction, Gabor filters, Euclidean distance.

Introduction

In recent years, with the development of information technology and the increasing need for security, intelligent personal identification has become a very important topic. Traditional methods for personal identification are based on token (a physical key, ID card) or knowledge (a secret password, PIN). These methods suffer from various problems. For example, ID cards may be forged or lost, and passwords may be forgotten or guessed. Biometric measurements (such as fingerprints or voiceprints) which are physiological or behavioral characteristics unique to an individual have the capability to reliably distinguish between an authorized person and an imposter. Generally, physiological and behavioral characteristics used in biometrics include the following: chemical composition of body odor; facial features and thermal emissions; features of the eye, i.e., retina and iris; fingerprints; palm-prints; hand geometry; handwritten signature; voiceprint; gait; gesture; etc. Of all these patterns, fingerprint identification and speaker recognition have received considerable attention over the last 25 years. Recently, with the changes of human's requirement, face recognition and iris based authentications have been studied widely. The human iris, as shown in Figure 1, has an extraordinary structure and provides abundant texture information.

The spatial patterns that are apparent in the iris are unique to each individual. Individual differences that exist in the development of anatomical structures in the body result in the uniqueness. In particular, the biomedical literature suggests that iris is as distinct as patterns of retinal blood vessels, but an iris image can be more easily obtained than a retina image. Compared with other biometrics (such as face, fingerprints, voiceprints, etc.), iris is more stable and reliable for identification. Since the iris is an overt body, iris recognition systems can be non-invasive to their users, which is a very important factor for practical applications.

Figure1. Example of an iris image

A general iris recognition algorithm includes image preprocessing, feature extraction, and classifier design. Section 2 describes image preprocessing which mainly involves iris localization, iris normalization and iris image enhancement and denoising. Feature extraction uses a bank of Gabor filters to capture both local and global details in an iris as a fixed length feature vector.

* Corresponding Author
E. mail: m24_kriti@yahoo.co.in

Iris localization

The iris is an annular part between the pupil (inner boundary) and the sclera (outer boundary). Both the inner boundary and the outer boundary of a typical iris can approximately be considered as circles. However, the two circles are usually not concentric. Iris localization by definition means to isolate the actual iris region in a digital eye image by detecting the inner and outer boundary of the iris. The eyelids and eyelashes normally occlude the upper and lower parts of the iris region. A technique is required to isolate and exclude these artifacts as well as locating the circular iris region.

Multi scale edge detection

Since an edge separates two different regions, an edge point is a point where the local intensity of the image varies rapidly more rapidly than in the neighbor points which are close from the edge: such a point could therefore be characterized as a local maximum of the gradient of the image intensity. The problem is that such a characterization is to be applied to differentiable images, and above all that it also detects all noise points. All techniques used so far to resolve the problem are based on smoothing the image first. However, a problem with smoothing arises: how much and which smoothing should one chooses? A strong smoothing will lead to the detection of less point while a lighter one will be more permissive. In this case every edge point of an image is characterized by a whole chain of the scale-space plane: the longer the chains are, the more important is the smoothing we impose, and the smaller number of edge points we will get.

In addition, this allows us to extract useful information about the regularity of the image at the edge point it characterizes. This can be very attractive in terms of a finer characterization of edge map.

Wavelet transform properties

Multi-scale edge detection can be formalized through a wavelet transform. Edges in images can be mathematically defined as local singularities. Until recently, the Fourier transforms was the main mathematical tool for analyzing singularities. However, the Fourier transform is global and not well adapted to local singularities. It is hard to find the location and spatial distribution of singularities with Fourier transforms. On the other hand, wavelet analysis is a local analysis; it is especially suitable for time-frequency analysis, which is essential for singularity detection. This was a major

motivation for the study of the wavelet transform in mathematics and in applied domains. With the growth of wavelet theory, the wavelet transforms have been found to be remarkable mathematical tools to analyze the singularities including the edges, and further, to detect them effectively. This idea is similar to that of Canny's approach which selects a Gaussian function as a smoothing function; while the wavelet-based approach chooses a wavelet function. Mallat et al. proved that the maxima of the wavelet transform modulus can detect the location of the irregular structures. One and two-dimensional signals can be reconstructed, with a good approximation, from the local maxima of their wavelet transform modulus.
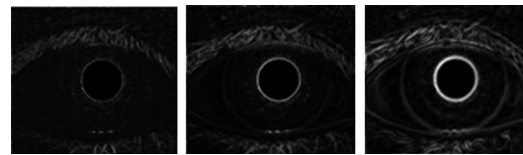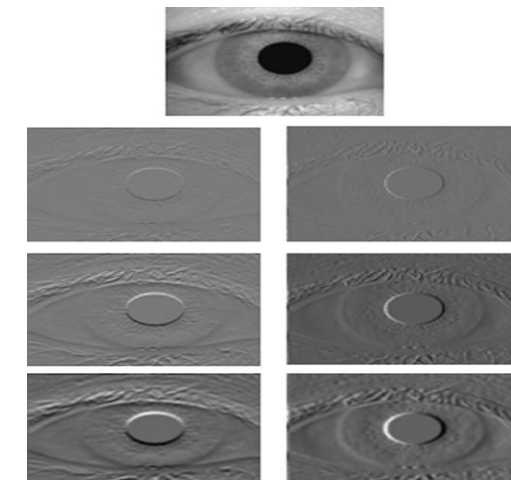

Fig.2. The modulus images $M(x, y, s)$ for $1<s<3$.

Fig. 3. Original image at the top, the first column on the left shows $Wh(x,y,s)$ for $1<s<3$, and the second column on the right shows $Wv(x,y,s)$ for $1<s<3$

The wavelet transform characterizes the local regularity of signals by decomposing signals into elementary building blocks that are well localized both in space and frequency. This not only explains the underlying mechanism of classical edge detectors, but also indicates a way of constructing optimal edge detectors under specific working conditions. A remarkable property of the wavelet transform is its ability to characterize the local regularity of functions. For an image $f(x, y)$, its edges correspond to singularities of $f(x, y)$, and

thus are related to the local maxima of the wavelet transform modulus. Therefore, the wavelet transform is an effective method for edge detection.

Multi-scale iris edge detection

The resolution of an image is directly related to the appropriate scale for edge detection. High resolution and a small scale will result in noisy and discontinuous edges; low resolution and a large scale will result in undetected edges. The scale controls the significance of edges to be shown. Edges of higher significance are more likely to be preserved by the wavelet transform across the scales. Edges of lower significance are more likely to disappear when the scale increases. Assume f (x, y) is a given image of size M×N. At each scale j with j >0 and S0f = f (x, y). The wavelet transform decomposes $S_{j-1}f$ into three wavelet bands: a low-pass band S_jf , a horizontal high-pass band W_j^Hf and a vertical high-pass band WjVf. The three wavelet bands (S_jf , W_j^Hf , W_j^Vf) at scale j are of size M×N, which is the same as the original image, and all filters used at scale j (j>0) are up-sampled by a factor of 2^j compared with those at scale zero. In addition, the smoothing function used in the construction of a wavelet reduces the effect of noise. Thus, the smoothing and edge detection steps are combined together to achieve the optimal result. The method of multi-scale edge detection is used to find the edges. This wavelet is non sub-sampled wavelet decomposition and essentially implements the discretized gradient of the image at different scales. At each level of wavelet transform the modulus M_jf of the gradients can be computed by

$$M_jf = \sqrt{|W_j^H f|^2 + |W_j^V f|^2}. \quad \ldots\ldots\ldots\ldots(1)$$

And the associated phase Ajf is obtained by

$$A_jf = \tan^{-1}(W_j^V / W_j^H). \quad \ldots\ldots\ldots\ldots(2)$$

The sharp variation points of the image f (x, y) smoothed by

S_jf (f (x, y) S_jf) are the points (x, y), where the modulus M_jf has a local maxima in the direction of the gradient given by A_jf. From Fig. 3, it can be observed that there is significant information about edge information in an eye image, with $W_h(x, y, s)$ eyelids and that the horizontal pupil's lines are clearer than outer boundary circle, and with $W_v(x, y, s)$ useful information about both pupil and outer boundary circles.
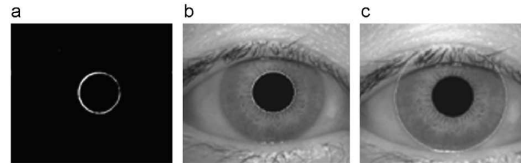

Fig. 4. Iris localized: (a) pupil edge map, (b) pupil detected, and (c) outer circle detected.

Detecting pupil and iris boundaries

To detect the iris and pupil boundaries an edge map has been detected first by using a multi-scale edge detection (Fig. 4).

The use of vertical coefficients for outer boundary edge detection will reduce the influence of the eyelids when performing a circular Hough transform because the eyelids are usually horizontally aligned. The Hough transform locates contours in an *n*-dimensional parameter space by examining whether they lie on curves of specified shape. For the iris outer or papillary boundaries and a set of recovered edge points (x_i, y_i), i = 1, . . . , n. A Hough transform is defined by

$$H(x_c, y_c, r) = \sum_{i=1}^{n} h(x_i, y_i, x_c, y_c, r),$$

where H(x_c,y_c,r) shows a circle through a point, the coordinates x_c, y_c, r define a circle by the following equation:

$$x_c^2 + y_c^2 + r^2 = 0. \quad \ldots\ldots\ldots\ldots.(3.1)$$

In the case of edge detection for iris boundaries Figs. 4(b) and (c) the above equation becomes:

$$(x_i - x_c)^2 + (y_i - y_c)^2 - r^2 = 0 \quad . \ldots\ldots\ldots..(3.2)$$

Isolating eyelids and eyelashes

Eyelids and eyelashes are isolated from the detected iris image

by considering them as noise because they degrade the performance of the system. The eyelids are isolated by first fitting a line to the upper and lower eyelid using the linear Hough transform. A horizontal line is then drawn which intersects with the first line at the iris edge that is closest to the pupil. A second horizontal line allows the maximum isolation of eyelid regions. A multi-scale edge detection is then used to create the edge map (Fig. 5), and only the horizontal gradient information is taken. If the maximum in the Hough space is lower than a set threshold, then no line is fitted, since this corresponds to non-occluding eyelids. Also, the lines are restricted to lie exterior to the pupil region and interior to the iris region. A thresholding operation is followed for detecting Eyelashes (Fig. 6)

Iris normalization

Once the iris region is segmented, the next stage is to normalize this part so as to enable the generation of the iris code and their comparisons. Since the variations in the eye, like optical size of the iris, position of pupil in the iris, and the iris orientation

change from person to person, it is required to normalize the iris image so that the representation is common to all, with similar dimensions.
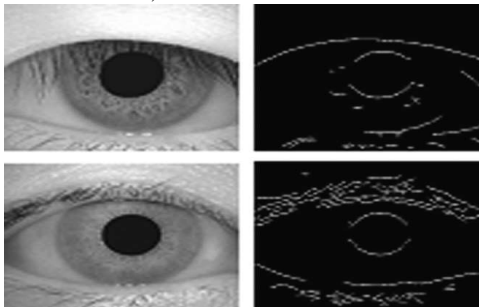

Fig. 5. Edges for eyelids detection: the first column on the left shows the original images and the second column on the right shows the edges detected using the horizontal coefficients Wh(x, y, 3).

The normalization process involves unwrapping the iris and

converting it into its polar equivalent. It is done using Daugman's Rubber sheet model (Fig. 7). The center of the pupil is considered as the reference point and a remapping formula is used to convert the points on the Cartesian scale to the polar scale. In this model a number of data points are selected along each radial line and this is defined as the radial resolution. The number of radial lines going around the iris region is defined as the angular resolution as in Figs. 8 and 9.
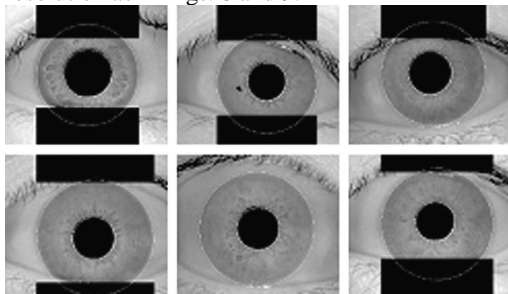

Fig. 6. Illustration of perfect iris localization, Black regions denote detected eyelid and eyelash regions
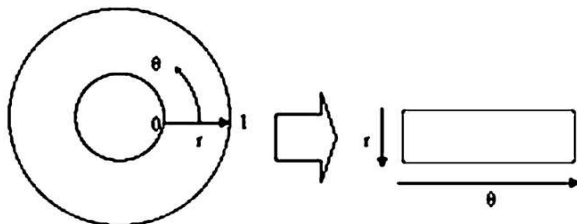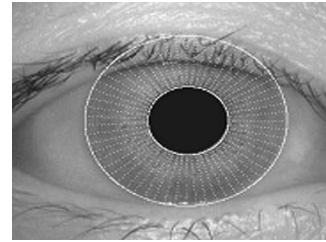

Fig. 7. Unwrapping the iris

Fig. 8. Draw of the normalized portion with radial resolution of 15 pixels, and angular resolution of 60 pixels.

Fig. 8. Normalized iris image.

Feature extraction

The iris has an interesting structure and presents plentiful texture information. So, it is attractive to search representation methods which can capture local crucial information in an iris. The distinctive spatial characteristics of the human iris are manifest at a variety of scales . For example, distinguishing

structures range from the overall shape of the iris to the distribution of tiny crypts and detailed texture. To capture this range of spatial detail, it is advantageous to make use of a multi-scale representation. Some works have used multi-resolution techniques for iris feature extraction [13–15] and have proven a high recognition accuracy. At the same time, however, it has been observed that each multi-resolution technique has its specification and situation in which it is suitable; for example, a Gabor filter bank has been shown to be most known multi-resolution method used for iris feature extraction and Daugman in his proposed iris recognition system demonstrated the highest accuracy by using Gabor filters. However, from the point of view of texture analysis one can observe that Gabor filter based methods analyze pretty well the texture orientations. We have analyzed iris textures in both horizontal and vertical directions especially that the iris has a rich structure with a very complex textures so that it makes sense to analyze the iris texture by combining all information extracted from iris region by considering all orientations in terms of horizontal and vertical details. To demonstrate this, we propose a new and combined multi-resolution iris feature extraction scheme by analyzing the iris using first wavelet maxima components and then applying a special Gabor filter bank to extract all dominant features.

Wavelet maxima components

Wavelet decomposition provides a very good approximation of images and natural setting for the multi-level analysis. Since wavelet transform maxima provide useful information about textures and edges analysis, we propose to use it here as a fast feature extraction by using the wavelet components. Wavelet maxima have been shown to work well in detecting edges which are likely key features in a query; moreover this

method provides useful information about texture features by using horizontal and vertical details.

To obtain wavelet decomposition pair of discrete filters H, G has been used. At each scale s, the algorithm decomposes the iris image $I(x, y)$ into $I(x, y, s)$, $W_v(x, y, s)$ and $W_h(x, y, s)$ as shown in Figs.10 and 11.

• $I(x, y, s)$: the image smoothed at scale s.

• $W_h(x, y, s)$ and $W_v(x, y, s)$ can be viewed as the two components of the gradient vector of the analyzed image $I(x, y)$ in horizontal and vertical direction, respectively.

In each scale s $(s<S)$ where S is the number of scales or decomposition, image $I(x, y)$ is smoothed by a low-pass filter:

$s = 0$,

$I(x, y, s+1) = I(x, y, s)(Hs, Hs)$. ………… (4)

And horizontal and vertical details are obtained, respectively,

By

$$W_h(x, y, s) = \frac{1}{\lambda_s} I(x, y, s)(G_s, D),$$ …………(5)

$$W_v(x, y, s) = \frac{1}{\lambda_s} I(x, y, s)(D, G_s).$$ …………(6)

• We denote by D the Dirac filter whose impulse response is

equal to 1 at 0 and 0 otherwise.

Table 1

Response to filters H, G

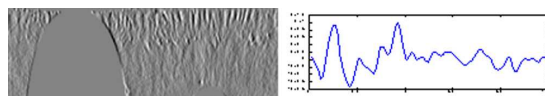| H	0	0	0.125	0.375	0.375	0.125	0
G	0	0	0	-2	2	0	0

Fig. 10. Wavelet maxima vertical component at scale 2 with intensities along specified column.
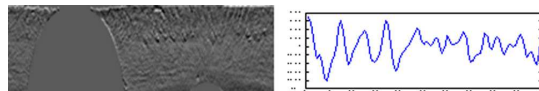

Fig. 11. Wavelet maxima horizontal component at scale 2 with intensities along specified column.

• We denote by $A(H,L)$ the separable convolution of the rows

and columns, respectively, of the image A with the $1-d$

filters H and L.

• G_s, H_s are the discrete filters obtained by putting 2^s-1 zeros between consecutive coefficients of H and G.

• λ_s, due to discretization, the wavelet modulus maxima of a step edge do not have the same amplitude at all scales as they should in a continuous model.

The constants λ_s compensate for this discrete effect.

Special Gabor filter bank

The two-dimensional Gabor Wavelets function $g(x, y)$ and its Fourier transform $G(u, v)$ can be defined as follows:

$$g(x, y) = \frac{1}{2\pi\sigma_x\sigma_y} \exp\left[-\frac{1}{2}\left(\frac{x^2}{\sigma_x^2} + \frac{y^2}{\sigma_y^2}\right) + 2\pi j W x\right],$$ ….(7)

$$G(u, v) = \exp\left[-\frac{1}{2}\left(\frac{(u-W)^2}{\sigma_u^2} + \frac{v^2}{\sigma_v^2}\right)\right],$$ ……(8)

where $\sigma_u = 1/2\pi\sigma x$ and $\sigma_v = 1/2\pi\sigma y$. A Gabor function can form a complete but non-orthogonal basis set and by expanding a signal using this basis provides a localized frequency description. A class of self-similar functions, referred to as Gabor wavelets in the following discussion, is now considered. Let $g(x,y)$ be the mother Gabor wavelet, then this self-similar filter dictionary can be obtained by appropriate dilations and rotations of $g(x,y)$ through the generating function:

$$g_{mn}(x, y) = a^{-m}G(x', y'),$$ ……………… (9)

$$x' = a^{-m}(x\cos\theta + y\sin\theta),$$ ………………(10)

$$y' = a^{-m}(-x\sin\theta + y\cos\theta),$$ ……………..(11)

where a>1, m, n =integer and $\theta=n\pi/k$ is the orientation (k is the number of orientations) and a^{-m} is the scale factor. The non-orthogonality of the Gabor wavelets implies that there is redundant information in the filtered images, and the following strategy is used to reduce this redundancy. Let U_l and U_h denote the lower and upper centre frequencies of interest. Let K be the number of orientations and S be the number of scales in the multi-resolution decomposition. Then the design strategy is to ensure that the half-peak magnitude support of the filter responses in the frequency spectrum touch each other as shown in Fig. 11 This results in the following formulas for computing the filter parameters σ_u and σ_v (and thus σ_x and σ_v).

$$a = (U_h/U_l)^{-1/(S-1)},$$ …………(12)

$$\sigma_u = \frac{(a-1)U_h}{(a+1)\sqrt{2\ln 2}},$$ ………..(13)

$$\sigma_v = \tan\left(\frac{\pi}{2k}\right)\left[U_h - 2\ln\left(\frac{\sigma_u^2}{U_h}\right)\right]$$
$$\times \left[2\ln 2 - \frac{(2\ln 2)^2\sigma_u^2}{U_h^2}\right]^{-1/2},$$

………(14)

Where $W = U_h$, and $m = 0, 1, \ldots, S - 1$. In order to eliminate
the sensitivity of the filter response to absolute intensity values, the real (even) components of the 2D Gabor filters are biased by adding a constant to make them zero mean.
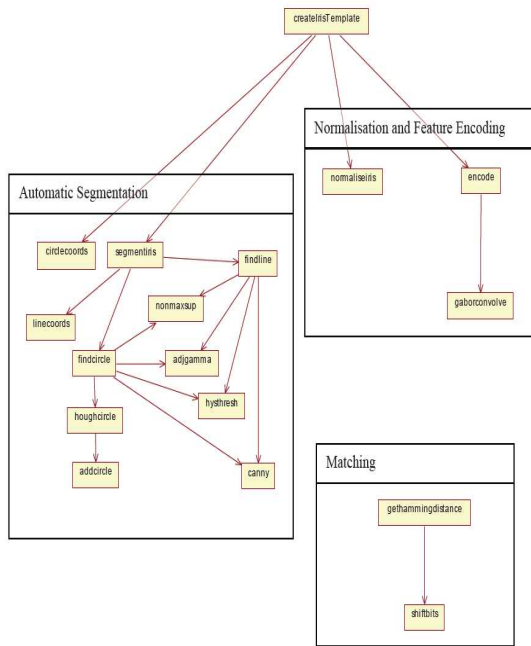

Fig.12.Flow for Create Iris Template

A feature vector can be constructed. For each filtered image
the statistical features of the image are computed such as the
mean and the variance (or standard deviation) μ_{mn} and μ_{mn}. In the experiments, we show that the best results are obtained if four scales $(S = 4)$ and six orientations $(K = 6)$ are used. The
resulting feature vector is as follows

$$f = [\mu_{0,0}, \sigma_{0,0}, \mu_{0,1}, \sigma_{0,1}, \ldots, \mu_{3,5}, \sigma_{3,5}].$$

……..(13)

After applying wavelet maxima components in the normalized
iris image and for each filtered image in both horizontal and
vertical direction for the five scales, a special Gabor filter bank has been used with four scales and six orientations, so that:

• For the horizontal details: wavelet maxima (five images) →
Gabor filters $(4 \times 6 \times 5) = 120$ images.
• For the vertical details: wavelet maxima (five images) →
Gabor filters $(4 \times 6 \times 5) = 120$ images.
With statistical features, mean and variance are calculated for
each image from $(120 \times 2) = 240$ images to obtain a feature vector of 480 elements.

Matching
It is very important to present the obtained vector in a binary code because it is easier to determine the difference between two binary code-words than between two number vectors. In fact, Boolean vectors are always easier to compare and to manipulate. We have applied a Hamming Distance matching algorithm for the recognition of two samples. It is basically an exclusive OR (XOR) function between two bit patterns. Hamming Distance is a measure, which delineate the differences, of iris codes. Every bit of presented iris code is compared to the every bit of referenced iris code, if the two bits are the same, e.g. two 1's or two 0's, the system assigns a value '0' to that comparison and if the two bits are different, the system assigns a value '1' to that comparison. The formula for iris matching is shown as follows:

$$HD = \frac{1}{N}\sum P_i \oplus R_i,$$

…………………..(14)

Where N is the dimension of feature vector, Pi is the ith component of the presented feature vector while Ri is the ith component of the referenced feature vector. The match ratio between two iris templates is given by

$$Ratio = \left(\frac{T_z}{T_b}\right) \times 100,$$

…………………(15)

where Tz is total number of zeros calculated by Hamming distance vector and Tb is the total number of bits in iris template.

Conclusion
In this paper, we have introduced a novel efficient multi scale approach for human iris recognition based on combined feature extraction methods by considering both the textural and topological features of an iris image which is invariant to translation, scale and rotation. The proposed algorithm yields superior performance when compared to the algorithms of Boles [14] and Tan [21], with lower complexity and high recognition rate, using lower complexity With Daugman's method [5] using CASIA database. All experimental results have demonstrated that the proposed method achieves high performance in both speed and accuracy.

This confirms that combined multi resolution feature extraction techniques truthfully perform iris recognition accuracy and our analysis and understanding are rational and practical.
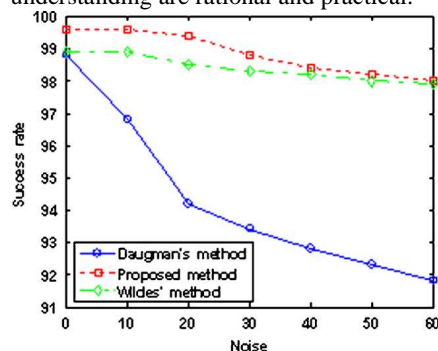

Fig. 14. Success rate of iris localization

References

1. R. Wildes, J. Asmuth, G. Green, S. Hsu, R. Kolczynski, J. Matey, S. McBride, A machine-vision system for iris recognition, Mach. Vision Appl. 9 (1996) 1–8.
2. M.S. Obaidat, B. Sadoun, Verification of computer users using keystroke dynamics, IEEE Trans. Syst. Man Cybernet. 27 (1997) 261–269.
3. J. Wayman, A. Jain, D. Maltoni, D. Maio, Biometric Systems, Technology, Design and Performance Evaluation, Springer, London, 2005.
4. F.H. Adler, Physiology of the Eye, Mosby, St. Louis, MO, 1965.
5. J.G. Daugman, High confidence visual recognition of persons by a test of statistical independence, IEEE Trans. Pattern Anal. Mach. Intell. 15(11) (1993) 1148–1161.
6. L. Flom, A. Safir, Iris recognition system, U.S. Patent 4 641 349, 1987.
7. L. Flom, A. Safir, Iris recognition system, U.S. Patent 4 641 394, 1987.
8. R. Johnson, Can iris patterns be used to identify people? Chemical and Laser Sciences Division LA-12 331-PR, Los Alamos Nat. Lab., Los Alamos, CA, 1991.
9. K. Bae, S. Noh, J. Kim, Iris feature extraction using independent component analysis, in: Proceedings of 4th International Conference on Audio- and Video-Based Biometric Person Authentication, 2003, pp. 838–844.
10. J. Daugman, Biometric personal identification system based on iris analysis, U.S. Patent 5 291 560, 1994.
11. J. Daugman, Demodulation by complex-valued wavelets for stochastic pattern recognition, Int. J.Wavelets Multi-Res. Info. Process. 1 (1) (2003) 1–17.
12. R. Sanchez-Reillo, C. Sanchez-Avila, Iris recognition with low template size, in: Proceedings of International Conference on Audio- and Video- Based Biometric Person Authentication, 2001, pp. 324–329.
13. R.P. Wildes, Iris recognition: an emerging biometrics technology, Proc. IEEE 85 (9) (1997) 1348–1363.
14. W. Boles, B. Boashash, A human identification technique using images of the iris and wavelet transform, IEEE Trans. Signal Process. 46 (1998) 1185–1188.
15. J.G. Daugman, How iris recognition works, IEEE Trans. Circuits Syst. Video Technol. 14 (1) (2004) 21–30.
16. S. Lim, K. Lee, O. Byeon, T. Kim, Efficient iris recognition through improvement of feature vector and classifier, ETRI J. 23 (2) (2001) 1–70.
17. C. Tisse, L. Martin, L. Torres, M. Robert, Person identification technique using human iris recognition, in: Proceedings of Vision Interface, 2002, pp. 294–299.
18. T. Tangsukson, J. Havlicek, AM-FM image segmentation, in: Proceedings of IEEE International Conference on Image Processing, 2000, pp. 104–107.
19. J. Havlicek, D. Harding, A. Bovik, The multi-component AM-FM image representation, IEEE Trans. Image Process. 5 (1996) 1094–1100.
20. B. Kumar, C. Xie, J. Thornton, Iris verification using correlation filters, in: Proceedings of 4th International Conference on Audio- and Video- Based Biometric Person Authentication, 2003, pp. 697–705.
21. L. Ma, T. Tan, Efficient iris recognition by characterizing key local variations, IEEE Trans. Image Process. 13 (2004) 739–750.
22. L. Ma, T. Tan, Y. Wand, D. Zhang, Personal identification based on iris texture analysis, IEEE Trans. Pattern Anal. Mach. Intell. 25 (12) (2003) 1519–1533.
23. A.K. Jain, F. Farrokhnia, Unsupervised texture segmentation using Gabor filters, Pattern Recogn. 24 (12) (1991) 1167–1186.
24. L. Pan, M. Xie, Research on iris image preprocessing algorithm, IEEE Int. Symp. Mach. Learning Cybernet. 8 (2005) 5220–5224.
25. S. Mallat, S. Zhong, Characterization of signals from multiscale edges, IEEE Trans. Pattern Anal. Mach. Intell. 14 (7) (1992) 710–732.

26. S. Mallat, A Wavelet Tour of Signal Processing, second ed., Academic Press, New York, 1998.

27. S. Mallat, Zero-crossing of a wavelet transform, IEEE Trans. Inf. Theory37 (4) (1991) 1019–1033.

28. B.S. Manjunath, W.Y. Ma, Texture features for browsing and retrieval of image data, IEEE Trans. Pattern Anal. Mach. Intell. 18(8) 1996.

29. A.K. Jain, Fundamentals of digital image processing, Prentice-Hall, Englewood Cliffs, NJ, 1989.

30. Chinese Academy of Sciences—Institute of Automation, Databaseof 756 Greyscale Eye Images, http://www.sinobiometrics.com_ Version 1.0, 2003.

31. C. Sanchez-Avila, R. Sanchez-Reillo, Iris-based biometric recognition using dyadic wavelet transform, IEEE Aerosp. Electron. Syst. Mag. 17 (2002) 3–6.